ResearchGate

See discussions, stats, and author profiles for this publication at: https://www.researchgate.net/publication/263165350

New palladium(II) complexes of 3-methoxysalicylaldehyde-4(N)- substituted thiosemicarbazones: Synthesis, spectroscopy, X-ray crystallography and DNA/protein binding study

ARTICLE *in* POLYHEDRON · FEBRUARY 2014

Impact Factor: 2.01

READS

45

1 AUTHOR:

R. Prabhakaran

Bharathiar University

52 PUBLICATIONS **965** CITATIONS

SEE PROFILE

Available from: R. Prabhakaran

Retrieved on: 13 January 2016

Polyhedron xxx (2014) xxx–xxx

Contents lists available at ScienceDirect

Polyhedron

journal homepage: www.elsevier.com/locate/poly

New palladium(II) complexes of 3-methoxysalicylaldehyde-4(*N*)-substituted thiosemicarbazones: Synthesis, spectroscopy, X-ray crystallography and DNA/protein binding study

P. Kalaivani [a], C. Umadevi [a], R. Prabhakaran [a,*], F. Dallemer [b], P.S. Mohan [a], K. Natarajan [a,*]

[a] Department of Chemistry, Bharathiar University, Coimbatore 641 046, India
[b] Laboratoire Chimie Provence-CNRS UMR6264, Université of Aix-Marseille I, II and III – CNRS, Campus Scientifique de Saint-Jérôme, Avenue Escadrille Normandie-Niemen, F-13397 Marseille Cedex 20, France

ARTICLE INFO

Article history:
Received 18 November 2013
Accepted 5 February 2014
Available online xxxx

Keywords:
Palladium(II) complexes
Thiosemicarbazones
X-ray crystallography
CT DNA binding
EB displacement study
BSA binding
Synchronous fluorescence spectroscopy

ABSTRACT

A series of 4(*N*)-substituted 3-methoxysalicylaldehyde thiosemicarbazone (**H_2L1**–**H_2L4**) were reacted with equimolar amount of $[PdCl_2(AsPh_3)_2]$ in ethanol/dichloromethane medium. The new complexes have been characterized by various spectroscopic techniques. The structure determination of the complexes [Pd(H-Msal-mtsc)($AsPh_3$)](**2**), [Pd(H-Msal-etsc)($AsPh_3$)](**3**) and [Pd(Msal-ptsc)($AsPh_3$)](**4**) by X-ray crystallography showed that the ligands **H_2L2** and **H_2L3** are coordinated as monobasic bidentate NS donor in the complexes **2** and **3** by forming a five member chelate ring. However, in the complex **4**, the ligand **H_2L4** bound to palladium as dibasic tridentate ONS donor by forming six and five member chelate rings. The binding ability of the palladium(II) precursor $[PdCl_2(AsPh_3)_2]$, ligands (**H_2L1**–**H_2L4**) and their corresponding complexes (**1**–**4**) with calf-thymus DNA (CT DNA) has been examined by photophysical studies, which revealed that the complexes bound to DNA through intercalation mode. The protein binding studies have been monitored by quenching of tryptophan and tyrosine residues in the presence of compounds by taking bovine serum albumin (BSA) as a model protein and the mechanism of quenching was found as static. The binding study results showed that the new complexes **1**–**4** possess better binding affinity than the starting precursor and ligands (**H_2L1**–**H_2L4**).

© 2014 Elsevier Ltd. All rights reserved.

1. Introduction

The chemistry of thiosemicarbazones has shown considerable interest being agents of diverse applications by exhibiting analytical, antimicrobial and antitumoral properties [1–3]. The presence of nitrogen and sulfur donor atoms in the ligand may be responsible for their potential biological activity. Nowadays metal based drugs have gained importance and become the burning topics in the experimental oncology [4]. Following the discovery of cisplatin *cis*-$[Pt(NH_3)Cl_2]$, interest on the discovery of new efficient antitumor complexes were increased. The clinical success of cisplatin is limited by significant side effects and acquired or intrinsic resistance. Therefore, much attention has been focused on designing more-efficacious, target-specific and less-toxic cytotoxic drugs. In general, platinum(II) complexes are thermodynamically and kinetically more stable than their analogs palladium(II) complexes. Palladium(II) complexes undergo aquation and ligand exchange reactions 10^5 times faster than the corresponding platinum(II) complexes [5]. A variety of palladium(II) complexes have been investigated as potential antitumor drugs [6–9] and some of the palladium(II) thiosemicarbazone complexes are tested and proved to be efficient compounds of pharmaceutical interest exerting cytotoxicity against the second most dangerous type of cancer called breast cancer, anti-mycobacterium tuberculosis activity [10], antimicrobial activity and antitrypanosomal activity [11–13]. Generally, the anti-cancer activity of the drugs is based on its interaction with the DNA of cancerous cell, which ultimately leads to programmed cell death. For the development of new metal-based therapeutics, detailed studies on their interactions with DNA in are anticipated [14,15]. In continuation with our investigation on palladium thiosemicarbazone complexes [16–20], herein we report the reactions of 3-methoxysalicylaldehyde-4(*N*)-substituted thiosemicarbazone (**H_2L1**–**H_2L4**) with palladium(II) complexes and their DNA/protein interactions.

* Corresponding authors. Tel.: +91 422 2428319; fax: +91 422 2422387.
E-mail addresses: rpnchemist@gmail.com (R. Prabhakaran), k_natraj6@yahoo.com (K. Natarajan).

http://dx.doi.org/10.1016/j.poly.2014.02.011
0277-5387/© 2014 Elsevier Ltd. All rights reserved.

2. Experimental

2.1. Materials and instrumentation

The ligands [**H_2L1**–**H_2L4**] and the palladium complex [$PdCl_2(AsPh_3)_2$] were synthesized according to the standard literature procedures [21,22]. All the reagents used were analaR grade, were purified and dried according to the standard procedure [23]. The syntheses, analytical and spectral characterization of the ligands (**H_2L1**–**H_2L4**) were reported by our group earlier [17]. Melting points were determined with Lab India instrument. Elemental analysis of complexes was performed on Vario EL III Elementar elemental analyzer. Electronic absorption spectra of the compounds were recorded using JASCO 600 spectrophotometer and emission measurements were carried out by using a JASCO FP-6600 spectrofluorometer. Nicolet Avatar Model FT-IR spectrophotometer was used to record the IR spectra (4000–400 cm^{-1}) of the ligands and the complexes as KBr pellets. ^1H NMR spectra were recorded in DMSO at room temperature with a Bruker 400 MHz instrument, chemical shift relative to tetramethylsilane. The chemical shifts are expressed in parts per million (ppm). CT DNA, BSA and ethidium bromide (EB) were obtained from Sigma Aldrich.

2.2. Synthesis of new palladium(II) complexes

2.2.1. Synthesis of [Pd(Msal-tsc)($AsPh_3$)] (**1**)

An ethanolic (25 ml) solution of [$PdCl_2(AsPh_3)_2$] (0.200 g; 0.253 mmol) was slowly added to 3-methoxysalicylaldehydethiosemicarbazone [H_2-Msal-tsc] (0.058 g, 0.253 mmol) in dichloromethane (25 ml). The mixture was allowed to stand for 4 days at room temperature.

A yellowish orange solid formed was filtered, washed with petroleum ether (60–80 °C). Yield: 51%. M.p. 225 °C. *Anal.* Calc. for $C_{27}H_{24}N_3O_2SPdAs$: C, 51.00; H, 3.80; N, 6.61; S, 5.04. Found: C, 50.98; H, 3.77; N, 6.59; S, 5.01%. FT-IR (cm^{-1}) in KBr: 1584 ($\nu_{C=N}$), 1310 (ν_{C-O}), 753 (ν_{C-S}), 1436, 1066, 694 cm^{-1} (for $AsPh_3$); UV–Vis (CH_2Cl_2), λ_{max}: 262 (30778) (intra-ligand transition); 332 (22160), 357 (19960), 418 (10360) nm ($dm^3\ mol^{-1}\ cm^{-1}$) (LMCT s → d); ^1H NMR (DMSO-d6, ppm): 8.25 (d (J = 14.1 Hz), 1H, CH=N), 3.61 (s, 3H, OCH_3), 6.49–7.71 (m, aromatic).

The very similar method was followed to synthesize other complexes.

2.2.2. Synthesis of [Pd(H-Msal-mtsc)($AsPh_3$)](**2**)

The complex **2** was prepared by the procedure as used for (**1**) with 3-methoxysalicylaldehyde 4(*N*)-methylthiosemicarbazone [H_2-Msal-mtsc] (0.060 g; 0.253 mmol) and [$PdCl_2(AsPh_3)_2$] (0.200 g; 0.253 mmol). The resulting solution was allowed to stand for 4 days at room temperature. The orange color solid obtained was recrystallized from CH_2Cl_2 and CH_3CN to yield orange red crystals which was filtered, washed with n-hexane and dried. Yield: 57%. M.p. 126 °C. *Anal.* Calc. for $C_{28}H_{27}N_3O_2SClPdAs$: C, 49.01; H, 3.96; N, 6.12; S, 4.67. Found: C, 48.98; H, 3.92; N, 6.09; S, 4.65%. FT-IR (cm^{-1}) in KBr: 3327 (ν_{OH}), 1547 ($\nu_{C=N}$), 1241 (ν_{C-O}), 734 (ν_{C-S}), 1458, 1072, 688 cm^{-1} (for $AsPh_3$); UV–Vis (CH_2Cl_2), λ_{max}: 263 (34536) nm ($dm^3\ mol^{-1}\ cm^{-1}$) (intra-ligand transition); ^1H NMR (DMSO-d6, ppm): 11.28 (s, 1H, OH), 8.36 (s, 1H, CH=N), 8.40 (s, 1H, $NHCH_3$), 3.61 (s, 3H, OCH_3), 6.49–7.71 (m, aromatic), 2.73 (d (J = 4.82), 3H, CH_3).

2.2.3. Synthesis of [Pd(H-Msal-etsc)($AsPh_3$)] (**3**)

The complex **3** was prepared by the procedure as used for (**1**) with 3-methoxysalicylaldehyde 4(*N*)-ethylthiosemicarbazone [H_2-Msal-etsc] (0.064 g; 0.253 mmol) and [$PdCl_2(AsPh_3)_2$] (0.200 g; 0.253 mmol). The red solid obtained was recrystallized from DMF to yield dark red crystals which was filtered, washed with n-hexane and dried. Yield: 67%. M.p. 231 °C. *Anal.* Calc. for $C_{29}H_{29}N_3O_2SClPdAs$: C, 49.73; H, 4.17; N, 6.01; S, 4.58. Found: C, 49.71; H, 4.15; N, 5.98; S, 4.57%. FT-IR (cm^{-1}) in KBr: 3318(ν_{OH}), 1578 ($\nu_{C=N}$), 1239 (ν_{C-O}), 733 (ν_{C-S}), 1457, 1082, 687 cm^{-1} (for $AsPh_3$); UV–Vis (CH_2Cl_2), λ_{max}: 267 (27821) nm ($dm^3\ mol^{-1}\ cm^{-1}$) (intra-ligand transition); ^1H NMR (DMSO-d6, ppm): 11.31 (s, 1H, OH), 8.58 (d (J = 4.40), 1H, CH=N), 7.68 (br s, 1H, NHC_2H_5), 3.78 (s, 3H, OCH_3), 6.79–7.67 (m, aromatic), 3.12–3.15 (m, 2H, CH_2), 1.05 (t, 3H, CH_3).

2.2.4. Synthesis of [Pd(Msal-ptsc)($AsPh_3$)] (**4**)

The complex **4** was prepared by the procedure as has been used for (**1**) with 3-methoxy salicylaldehyde 4(*N*)-phenylthiosemicarbazone [H_2-Msal-ptsc] (0.076 g; 0.253 mmol) and [$PdCl_2(AsPh_3)_2$] (0.200 g; 0.253 mmol). Dark red crystals obtained were filtered and washed with n-hexane and dried. Yield: 71%. M.p. 242 °C. *Anal.* Calc. for $C_{33}H_{28}N_3O_2SPdAs$: C, 55.67; H, 3.96; N, 5.90; S, 4.50. Found: C, 55.65; H, 3.95; N, 5.88; S, 4.48%. FT-IR (cm^{-1}) in KBr: 1591 ($\nu_{C=N}$), 1312 (ν_{C-O}), 738 (ν_{C-S}), 1431, 1078, 689 cm^{-1} (for $AsPh_3$);UV–Vis (CH_2Cl_2), λ_{max}: 263 (34647) ($dm^3\ mol^{-1}\ cm^{-1}$) (intra-ligand transition); 353 (26070), 409 (17320) nm ($dm^3\ mol^{-1}\ cm^{-1}$) (LMCT s → d); ^1H NMR (DMSO-d6, ppm): 8.67 (d (J = 13.4), 1H, CH=N), 9.41 (s, 1H, NHPh), 3.65 (s, 3H, OCH_3), 6.54–7.74 (m, aromatic).

2.3. X- ray crystallography

Single crystal data collections and corrections for the new **Pd(II)** complexes **2**, **3** and **4** were done at 293 K with CCD Kappa Diffractometer using graphite mono chromated Mo Kα (λ = 0.71073 Å) radiation [24]. The structural solutions were done by using SHELXTL-97 [25] and refined by full matrix least square on F^2 using SHELXL-97 [26].

2.4. Binding studies

2.4.1. DNA binding study

All of the experiments involving the binding of the compounds with CT DNA were carried out in deionised water with tris(hydroxymethyl)-aminomethane (Tris, 5 mM) and sodium chloride (50 mM) and adjusted to pH 7.2 with hydrochloric acid at room temperature. Various concentrations of CT-DNA (0–50 μM) was added to the compounds (10 μM). Absorption spectra were recorded after equilibrium at 20 °C for 10 min. The intrinsic binding constant K_b was determined by using Stern–Volmer equation (1) [27,28].

$$([DNA]/[\varepsilon_a - \varepsilon_f]) = [DNA]/[\varepsilon_b - \varepsilon_f] + 1/K_b[\varepsilon_b - \varepsilon_f] \quad (1)$$

The absorption coefficients ε_a, ε_f, and ε_b correspond to A_{obsd}/[compound], the extinction coefficient for the free compound and the extinction coefficient for the compound in the fully bound form, respectively. The slope and the intercept of the linear fit of the plot of $[DNA]/[\varepsilon_a - \varepsilon_f]$ versus [DNA] give $1/[\varepsilon_a - \varepsilon_f]$ and $1/K_b[\varepsilon_b - \varepsilon_f]$, respectively. The intrinsic binding constant K_b can be obtained from the ratio of the slope to the intercept. It can be determined by monitoring the changes in the absorbance in the intra ligand band at the corresponding λ_{max} with increasing concentration of DNA and is given by the ratio of slope to the Y intercept in plots of $[DNA]/(\varepsilon_a - \varepsilon_f)$ versus [DNA].

2.4.2. Competitive binding with ethidium bromide

In order to know the mode of attachment of CT DNA to the complexes fluorescence quenching experiments of EB–DNA were carried out by adding 0–50 μM compounds containing 10 μM EB,

10 μM DNA and tris-buffer (pH 7.2). Before measurements, the system was shook and incubated at room temperature for ~5 min. The emission was recorded at 530–750 nm. The quenching extents of complexes were evaluated qualitatively by employing Stern–Volmer equation (2).

$$I_0/I = K_{sv}[Q] + 1 \quad (2)$$

where I_0 is the emission intensity in the absence of compound, I is the emission intensity in the presence of compound, K_{sv} is the quenching constant, and [Q] is the concentration of the compound. The K_{sv} values have been obtained as a slope from the plot of I_0/I versus [Q].

2.4.3. Bovine serum albumin binding study

The protein binding study was performed by tryptophan fluorescence quenching experiments using bovine serum albumin (BSA, 10 μM) as the substrate in phosphate buffer (pH 7.2). Quenching of the emission intensity of tryptophan residues of BSA at 346 nm (excitation wavelength at 276 nm) was monitored using compound as quenchers with increasing compound concentration. The possible quenching mechanism has been interpreted using the following Stern–Volmer equation (3), the ratio of the fluorescence intensity in the absence of (I_0) and in the presence of (I_{corr} – corrected fluorescence intensity) the quencher is related to the concentration of the quencher [Q] by a coefficient K_{sv}.

$$I_0/I_{corr} = 1 + K_{SV}[Q] \quad (3)$$

In order to correct the inner filter effect the following equation (4), is used.

$$F_{corr} = F_{obs} * 10^{\frac{A_{exc}+A_{em}}{2}} \quad (4)$$

where F_{corr} is the corrected fluorescence value, F_{obs} the measured fluorescence value, A_{exc} the absorption value at the excitation wavelength, and A_{em} the absorption value at the emission wavelength [29].

The binding constant (K_b) and the number of binding sites (n) can be determined according to the Scatchard equation (5) [30].

$$\log\,[(I_0 - I)/I] = \log K_b + n \log [Q] \quad (5)$$

where, in the present case, K_b is the binding constant for the quencher–fluorophore interaction and n is the number of binding sites per albumin molecule, which can be determined by the slope and the intercept of the double logarithm regression curve of log $[(I_0 - I)/I]$ versus log [Q]. Synchronous fluorescence spectra of BSA with various concentrations of complexes (0–50 μM) were obtained from 300 to 500 nm when $\Delta\lambda$ = 60 nm and from 290 to 500 nm when $\Delta\lambda$ = 15 nm. The excitation and emission slit widths were 5 and 6 nm, respectively. Fluorescence and synchronous measurements were performed by using a 1 cm quartz cell on a JASCO FP 6500 spectrofluorometer.

3. Results and discussion

3.1. Synthesis and characterization

The reaction of $[PdCl_2(AsPh_3)_2]$ with an equimolar amount of various 4(*N*)-substituted thiosemicarbazones (**H_2L1**–**H_2L4**) in 1:1 ethanol/dichloromethane resulted in the formation of new complexes (Scheme 1), the analytical data of which confirmed the stoichiometry of the complexes (**1**–**4**). The structure of the complexes **2**–**4** was confirmed by X-ray crystallographic study and attempts were made to grow single crystals of complex **1** in various organic solvents were unsuccessful. The complexes are soluble in common organic solvents such as dichloromethane, chloroform, benzene, acetonitrile, ethanol, methanol, dimethylformamide and dimethylsulfoxide.

3.2. Spectroscopic studies

In order to confirm the new complex formation the IR spectra of the ligands (**H_2L1**–**H_2L4**) and the corresponding complexes **1**–**4** were recorded. A band in the region 3339–3458 cm^{-1} due to the presence of –OH group in the free ligands (**H_2L1**–**H_2L4**) was completely disappeared in the IR spectra of complexes **1** and **4** indicating the coordination of phenolic oxygen to palladium after deprotonation. This was further supported by the increase in the phenolic C—O stretching frequency from 1272 to 1310 cm^{-1} and 1273 to 1312 cm^{-1} in the complexes **1** and **4** respectively [31]. However, the $\nu_{(O-H)}$ stretching frequency found at 3327 and 3318 cm^{-1} in the complexes **2** and **3**, indicate the non-participation of phenolic oxygen in coordination. The ligands showed a strong absorption at 1536–1593 cm^{-1} due to the presence of azomethine group and this has been shifted to 1547–1591 cm^{-1} in all the complexes indicating the coordination of azomethine nitrogen to metal atom [32,33]. A sharp band observed at 771–795 cm^{-1} ascribed to $\nu_{(C=S)}$ in the ligands was completely disappeared in the spectra of all the new complexes and the appearance of a new band at 733–753 cm^{-1} due to $\nu_{(C-S)}$ indicating the enolisation of NH—C≡S group and subsequent coordination through the deprotonated sulfur atom [16,34]. In addition, the characteristic absorption bands corresponding to triphenylarsine were also present in the expected region [19,20]. The electronic spectra of the complexes have been recorded in dichloromethane and they displayed bands in the region around 262–418 nm. The bands appeared in the region 262–267 nm have been assigned to intra ligand transition [35] and the bands around 332–418 nm have been assigned to ligand to metal charge transfer transition [35a,36]. The ^{1}H NMR spectra of **H_2L1**–**H_2L4** and the corresponding complexes **1**–**4** recorded in DMSO showed all the expected signals. In the spectra of **H_2L1**–**H_2L4**, a singlet appeared in the range 9.13–10.00 ppm has been assigned to N(2)HCS group [37]. However, in the spectra of the new complexes (**1**–**4**), there was no resonance attributable to N(2)H, indicating the coordination of ligands in the anionic form after deprotonation at N(2). A sharp singlet appeared at 11.34–11.76 ppm corresponding to the phenolic –OH group in the free ligands was completely disappeared in **1** and **4** confirming the involvement of phenolic oxygen in coordination. However, in the spectra of **2** and **3** the appearance of a singlet at 11.28 and 11.31 ppm respectively indicated the non-participation of phenolic oxygen in coordination [38]. The aromatic protons corresponding to the presence of coordinated ligands and triphenylarsine were appeared as multiplet at 6.49–7.74 ppm, and a singlet corresponding to the –OCH_3 group also found at 3.61–3.78 ppm [17]. Two singlets observed at 8.37–8.40 and 8.37–9.40 ppm has been assigned to azomethine and terminal –NH protons of the ligands [16]. Two broad singlets were observed at 7.81 and 8.02 ppm corresponding to NH_2 protons of the **H_2L1**. The spectrum of **2** showed a singlet at 8.36 ppm corresponding to azomethine proton and the same has been observed as a doublet at 8.25–8.67 ppm for **1**, **3** and **4** [17]. In the spectra of the complexes **2**, **3** and **4**, a sharp singlet observed around 7.68–9.41 ppm assigned the presence of terminal –NH protons of substituted thiosemicarbazone ligands. Further, a doublet was observed at 2.99 and 2.73 ppm in **H_2L2** and **2** corresponding to the presence of terminal CH_3 protons and a triplet observed at 1.13 and 1.05 ppm corresponding to a terminal CH_3 group of **H_2L3** and **3**. In addition, a multiplet appeared at δ 3.12–3.58 ppm in **H_2L3** and **3** which was assigned to the terminal methylene protons of ethyl group [17].

3.3. X-ray crystallography

Though the elemental analyses, infrared and ^{1}H NMR spectral data gave some basic information about the molecular formulae

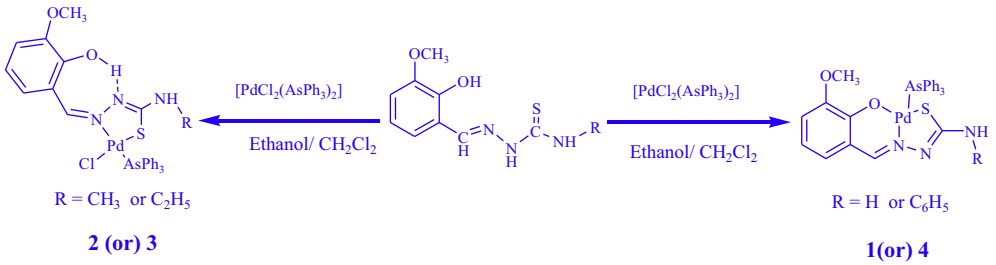

Scheme 1. Preparation of new palladium(II) complexes.

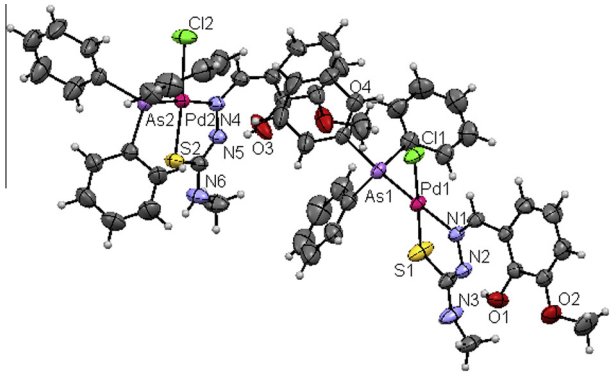

Fig. 1. ORTEP diagram with atom numbering scheme for **2** showing two independent molecules (thermal ellipsoids at 50% probability level).

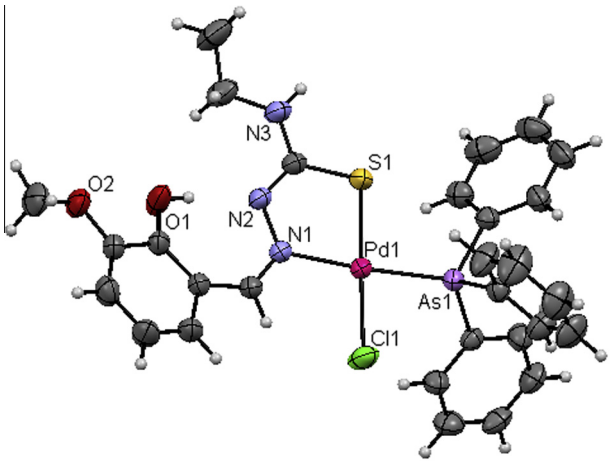

Fig. 3. ORTEP diagram with atom numbering scheme for **3** as thermal ellipsoids at 50% probability level.

of the complexes and the exact structure of them were not established. Hence, the exact structure of the complexes was solved by X-ray crystallography. The ORTEP diagram with the atom labeling scheme, hydrogen bonding interaction and packing diagram of the unit cell for the complexes **2**–**4** are displayed in Figs. 1–5 and S1--S3 (Supporting information). A summary of the structure refinement and selected geometrical parameters (inter-atomic distances and angles) are given in Tables 1 and 2 respectively. The hydrogen bond distances are given in the Tables S1 and S2.

Complex **2** crystallized in triclinic space group $P\bar{1}$. There are two crystallographic independent molecules present in the unit cell. The complex contains a bidentate monobasic thiosemicarbazone with NS chelation, by forming a five member ring with bite angles S1–Pd1–N1 and S2–Pd2–N4 of 83.24(7)° and 83.53(6)° respectively. The Pd–N, Pd–S, Pd–Cl and Pd–As bond lengths are quite normal as found in other square planar **Pd(II)** complexes [17,20]. The *cis* angles, Cl1–Pd1–As1 89.78(2)° and Cl2–Pd2–As2 88.35(2)° are less than 90°, whereas the other *cis* angles, S1–Pd1–As1 91.52(2)°, S2–Pd2–As2 91.93(2)°, Cl1–Pd1–N1 95.66(6)° and Cl2–Pd2–N4 96.44(6)° are greater than 90°. The *trans* angles As1–Pd1–N1 172.67(6)°, As2–Pd2–N4 174.66(6)°, Cl1–Pd1–S1 177.43(4)° and Cl2–Pd2–S2 174.61(4)° deviate from linearity leading to distortion in the geometry around palladium(II). Complex **3** crystallized in monoclinic space group $P21/c$ with mono basic bidentate chelation of the ligand. The ligand coordinated to palladium through thiolate sulfur (Pd–S bond distance of 2.241(7) Å), and the N1 hydrazinic nitrogen atom (Pd–N bond distance of 2.090(19) Å). All the bond lengths fall in the range of reported values [17,20]. The As(1)–Pd(1)–N(1) bond angle [175.76(5)°] and Cl(1)–Pd(1)–S(1) bond angle [174.16(3)°] deviate considerably from the ideal angle of 180°. The variation in bond angles in the complexes indicates considerable distortion from square planar geometry around palladium. Complex **4** crystallized in monoclinic space group $P21$ and in this complex, the ligand coordinated to palladium through thiolate sulfur (Pd–S bond distance of 2.239(1) Å), phenolic oxygen (Pd–O bond distance of 2.025(3) Å) and the nitrogen atom (Pd–N bond distance of 2.010(3) Å). The remaining binding site is occupied by the triphenylarsine unit (Pd–As(1) bond distances of 2.378(3) Å) with a bite angle [S(1)–Pd(1)–N(1)] of 84.67(9)° and acted as dibasic tridentate ligand. The [S(1)–Pd(1)–O(1)] bond angle [177.90(7)°] and

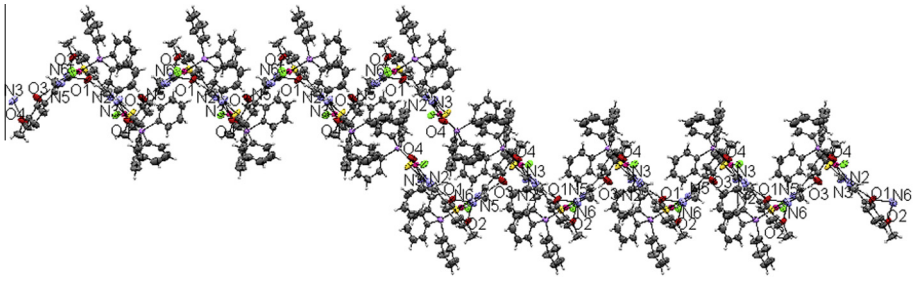

Fig. 2. ORTEP diagram of **2** with hydrogen bonding.

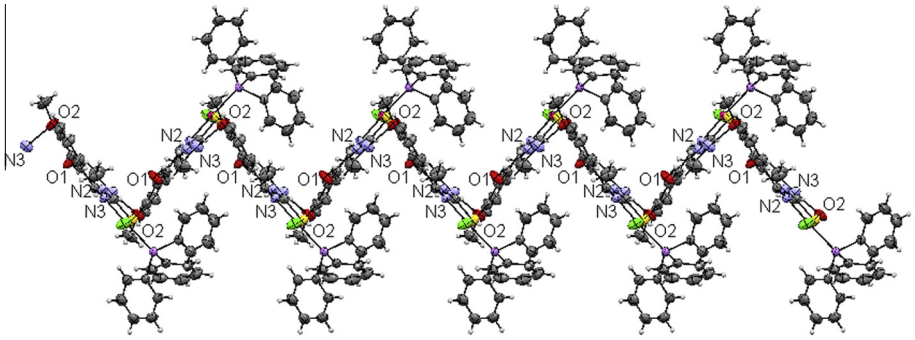

Fig. 4. ORTEP diagram of **3** with hydrogen bonding.

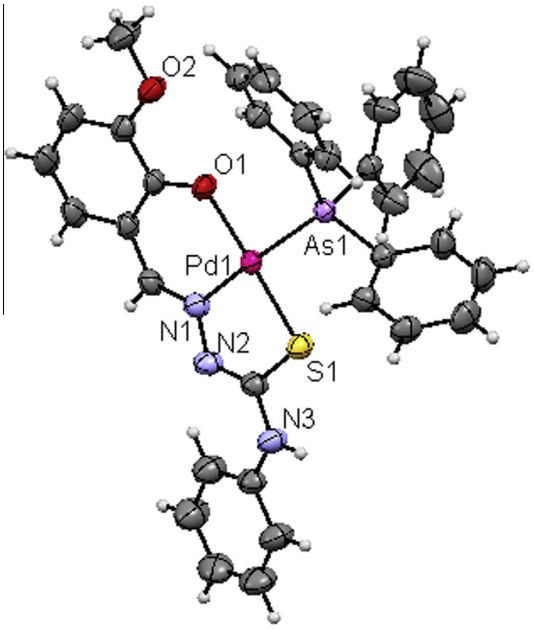

Fig. 5. ORTEP diagram with atom numbering scheme for **4** as thermal ellipsoids at 50% probability level.

[As(1)–Pd(1)–N(1)] bond angle [172.17(8)°] deviate considerably from the ideal angle of 180° causing significant distortion in the square planar geometry of the complexes.

In the complex **2**, two crystallographic independent molecules present in the unit cell. It is stabilized by two intra hydrogen bonding and two inter molecular hydrogen bonding networks with neighboring molecules. Though the hydroxyl groups (Phenolic –OH) O3 and O1 (H-donor) does not take part in coordination, it is involved in intramolecular hydrogen bonding interactions with adjacent hydrazinic nitrogen atoms N2 and N5 (H-acceptor). The terminal –N3H group (H-donor) of first unit is involved in intermolecular hydrogen bonding interaction with the methoxy oxygen atom O(4) (H-acceptor) of neighboring unit and the terminal –N6H group (H-donor) of second unit is involved in intermolecular hydrogen bonding interaction with the phenolic oxygen atom O1 (H-acceptor) of another unit. In addition, the complex **2** is having non-covalent interaction(s) between the terminal nitrogen (N6) and methoxy oxygen (O2) (Table S1 and Fig. 2). The complex **3** is stabilized by one intra molecular and two inter molecular hydrogen bonding interactions. The uncoordinated phenolic –O1 H1 (H-donor) is involved in intramolecular hydrogen bonding interaction with adjacent hydrazinic nitrogen N2 (H-acceptor). First intermolecular hydrogen bonding was observed between the terminal –N3H3A group (H-donor) and methoxy oxygen O(4) (H-acceptor) of neighboring unit and second intermolecular hydrogen bonding was observed between methoxy oxygen O(4) (H-acceptor) and the terminal –N3H3A group (H-donor) of neighboring unit (Table S2). The result is the assembly of discrete complexes into supramolecular 1D chain. This allows the assembly of individual 1D chain into a *zigzag* supramolecular network (Fig. 4).

3.4. DNA binding studies

DNA binding is one of the main properties in pharmacology for evaluating the anticancer property of any new compound, and hence, the interaction between DNA and metal complexes is of paramount importance in understanding the mechanism. Thus, the mode and propensity for binding of the palladium(II) starting material $[PdCl_2(AsPh_3)_2]$ (**Pd(II)**), ligands (**H_2L1**–**H_2L4**) and their corresponding new palladium(II) complexes **1**–**4** to CT DNA were studied by electronic absorption and fluorescence quenching experiments. The absorption spectra of the new complexes **1**–**4** and (**Pd(II)**), (**H_2L1**–**H_2L4**) are given in Figs. 6 and S4 respectively. In the absorption titrations, (**Pd(II)**) and (**H_2L1**–**H_2L4**) absorption bands were exhibited absorption at 262 and 263 nm. The electronic spectra of the compounds are slightly different from each other only in their visible region. When the concentration of DNA was increased, the intensity of the absorption bands around 262–266 nm corresponding to (**Pd(II)**) and (**H_2L1**–**H_2L4**) was affected by resulting in hypochromism of 53.10%, 85.36%, 88.85%, 89.73% and 73.37% respectively with red shift. The absorption spectra of complex **1** mainly consist of four resolved bands [Intra ligand (IL) and charge transfer (CT) transitions] centered at 262 nm (IL) 332, 357 and 418 nm (CT). As the DNA concentration is increased, the hypochromism of 88.80% with a red shift of 3 nm was observed in the intra ligand band. The CT bands at 332, 357 and 418 nm showed 3.05%, 3.85% and 8.59% hyperchromism respectively without any shift in the absorption maxima. For complex **2**, upon addition of DNA, the intra ligand band at 263 nm exhibited hypochromism of 97.84% with a red shift of 2 nm. Similarly, complexes **3** exhibited hypochromism (IL) at 263 (98.35%) with a red shift of 3 nm. Complex **4** showed hypochromism of 89.72% with a blue shift of 13 nm in the intra ligand band. The CT bands at 353 and 409 nm showed 17.36% and 28.48% hyperchromism respectively without any shift in the absorption maxima. Normally, a compound can bind to DNA through intercalation mode results in hypochromism with or without a small red or blue shift, due to a strong stacking interaction between the planar aromatic chromophore of the compound and the base pairs of DNA [39]. Hence, the observed hypochromic effect in the intra ligand band suggested that the test compounds bind to CT-DNA via intercalation mode. The intrinsic binding constant K_b was determined by using Stern–Volmer equation (1) [27,28]. From the binding constant

Table 1
Crystallographic data of new **Pd(II)** thiosemicarbazone complexes.

	[Pd(H-Msal-mtsc)Cl(AsPh$_3$)] (**2**)	[Pd(H-Msal-etsc)Cl(AsPh$_3$)] (**3**)	[Pd(MSal-ptsc)(AsPh$_3$)](**4**)
Empirical formula	$C_{56}H_{54}As_2Cl_2N_6O_4Pd_2S_2$	$C_{29}H_{29}As_1Cl_1N_3O_2Pd_1S_1$	$C_{33}H_{28}As_1N_3O_2Pd_1S_1$
Formula weight	1372.71	700.38	711.96
Crystal system	triclinic	monoclinic	monoclinic
Space group	$P\bar{1}$	$P21/c$	$P21$
Wavelength (Å)	0.71073	0.71073	0.71073
Temperature (K)	293	293	293
a (Å)	9.9643(1)	14.9529(3)	12.0780(1)
b (Å)	15.9065(2)	10.3520(2)	8.0155(1)
c (Å)	18.6352(3)	19.1112(3)	15.8123(2)
α (°)	103.974(1)	90	90
β (°)	91.1084(6)	103.138(1)	102.782(10)
γ (°)	96.681(1)	90	90
V (Å^3)	2843.30(6)	2880.84(9)	1492.87(3)
Crystal size (mm)	0.14 × 0.18 × 0.3	0.14 × 0.18 × 0.3	0.10 × 0.18 × 0.26
Z value	2	4	2
Limiting indices	$-11 \leqslant h \leqslant 12$, $-21 \leqslant k \leqslant 20$, $-23 \leqslant l \leqslant 25$	$-15 \leqslant h \leqslant 19$, $-13 \leqslant k \leqslant 13$, $-24 \leqslant l \leqslant 21$	$-16 \leqslant h \leqslant 16$, $-10 \leqslant k \leqslant 8$, $-17 \leqslant l \leqslant 21$
*D*calc	1.603	1.615	1.584
Reflections collected/unique	34072/11306[R_{int} 0.0329]	31191/5288[R_{int} 0.0443]	14352/6582[R_{int} 0.0312]
Theta range for data collection (°)	1.13–29	2.31–27.38	1.93–28.99
F(000)	1376	1408	716
Goodness-of-fit (GOF) on F^2	1.054	1.025	0.553
Refinement method	full-matrix least-squares on F^2	full-matrix least-squares on F^2	full-matrix least-squares on F^2
μ(Mo Kα)	2.005	1.981	1.826
Completeness to theta $2\theta_{max}$ (°)	29	27.38	28.99
Data/restraints/parameters	14361/0/667	6443/0/346	7244/1/371
Final R indices [$I > 2\sigma(I)$]	R_1 = 0.0373, wR_2 = 0.0817	R_1 = 0.0295, wR_2 = 0.0642	R_1 = 0.0278, wR_2 = 0.0705
R indices (all data)	R_1 = 0.0559, wR_2 = 0.0898	R_1 = 0.046, wR_2 = 0.07	R_1 = 0.0334, wR_2 = 0.0752
Largest difference in peak and hole (e Å^{-3})	0.553 and −0.738	0.567 and −0.925	0.747 and −0.838

Table 2
Selected bond lengths (Å) and angels (°) for **Pd(II)** thiosemicarbazone complexes.

Atoms	[Pd(H-Msal-mtsc)Cl(AsPh$_3$)](**2**)	[Pd(H-Msal-etsc)Cl(AsPh$_3$)](**3**)	[Pd(MSal-ptsc)(AsPh$_3$)](**4**)
Pd1–S1	2.241(1)	2.241(7)	2.239(1)
Pd1–As1	2.367(3)	2.368(3)	2.378(3)
Pd1–O1	–	–	2.025(3)
Pd1–N1	2.081(2)	2.090(19)	2.010(3)
Pd1–Cl1	2.326(7)	2.335(7)	–
Pd2–S2	2.234(7)		
Pd2–As2	2.359(3)		
Pd2–N4	2.093(2)		
Pd2–Cl2	2.331(8)		
S1–Pd1–As1	91.52(2)	92.49(19)	92.98(2)
S1–Pd1–O1	–	–	177.90(7)
S1–Pd1–N1	83.24(7)	83.72(5)	84.67(9)
As1–Pd1–O1	–	–	89.09(7)
As1–Pd1–N1	172.67(6)	175.76(5)	172.17(8)
O1–Pd1–N1	–	–	93.32(11)
Cl1–Pd1–N1	95.66(6)	95.71(5)	–
Cl1–Pd1–As1	89.78(2)	87.86(2)	–
Cl1–Pd1–S1	177.43(4)	174.16(3)	–
S2–Pd2–As2	91.93(2)		
S2–Pd2–N4	83.53(6)		
As2–Pd2–N4	174.66(6)		
Cl2–Pd2–N4	96.44(6)		
Cl2–Pd2–As2	88.35(2)		
Cl2–Pd2–S2	174.61(4)		

values (insects of Figs. 6 and S4; Table 3), it is inferred that there are intense interactions of new complexes **1**–**4** with DNA, which are stronger than that of (**Pd(II)**) and (**H_2L1**–**H_2L4**) and among the complexes, **3** exhibited better binding activity.

3.4.1. Competitive studies with ethidium bromide

DNA binding study point out that the new palladium(II) complexes effectively bind to DNA. Further, this has been confirmed by ethidium bromide displacement experiments. In general, the intrinsic fluorescence intensity of DNA is very low, and that of EB in Tris–HCl buffer is also not high due to quenching by the solvent molecules. However, on addition of DNA to EB, the fluorescence intensity of EB will be enhanced because of its intercalation into the DNA. Thus, EB can be used to probe the interaction of compounds with DNA. The fluorescence intensity of EB can be quenched by the addition second DNA binding molecule by either replacing the EB and/or by accepting the excited-state electron of the EB through a photoelectron transfer mechanism. The fluorescence spectra of EB were measured using an excitation wavelength of 620 nm, and the emission range was set between 550 and

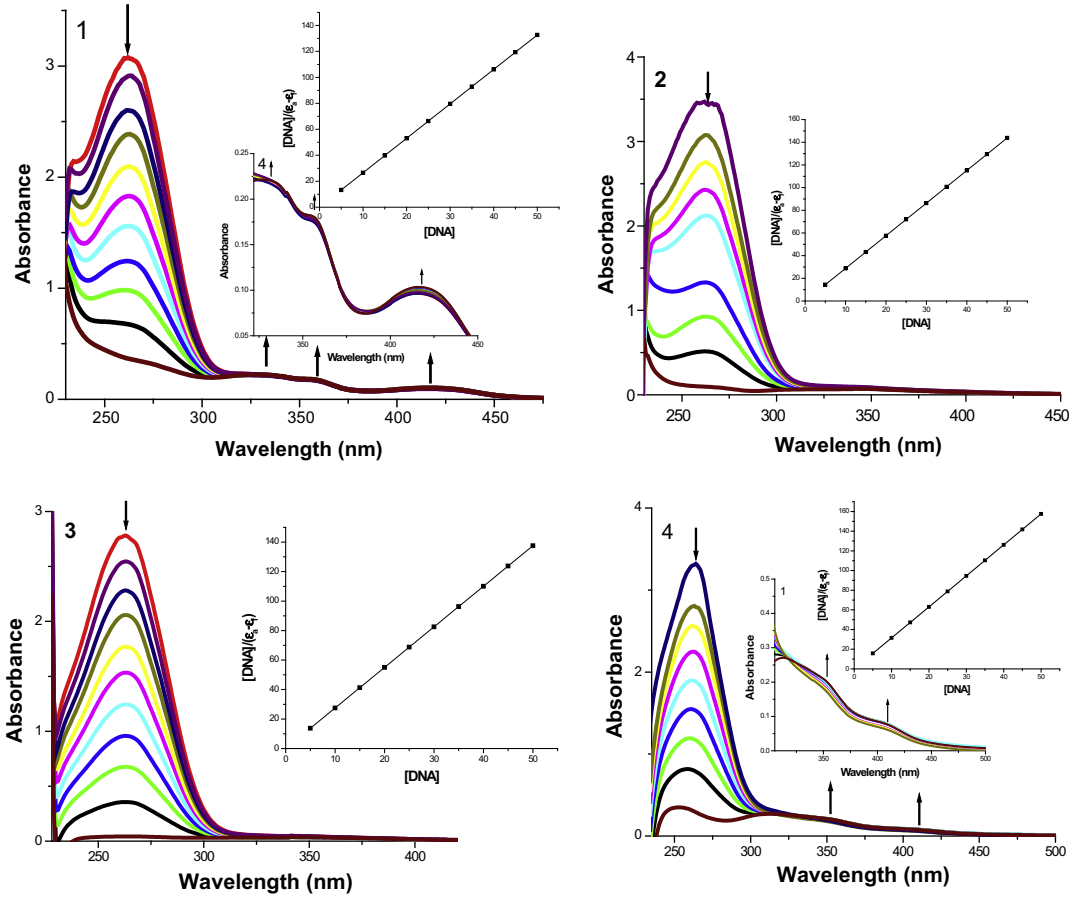

Fig. 6. Absorption titration spectra of fixed concentration (10 μM) of complexes **1–4** with increasing concentrations (0–50 μM) of CT-DNA (phosphate buffer, pH 7.2).

Table 3
The K_b and K_{sv} values for the interactions of compounds with CT-DNA.

Complex	K_b (M^{-1})	K_{sv} (M^{-1})
(**H_2L1**)	$1.34 \pm 0.32 \times 10^3$	$2.31 \pm 0.26 \times 10^3$
(**H_2L2**)	$1.41 \pm 0.26 \times 10^3$	$3.36 \pm 0.12 \times 10^3$
(**H_2L3**)	$1.55 \pm 0.21 \times 10^3$	$3.52 \pm 0.18 \times 10^3$
(**H_2L4**)	$1.36 \pm 0.31 \times 10^3$	$2.75 \pm 0.21 \times 10^3$
Pd(II)	$1.23 \pm 0.25 \times 10^3$	$1.76 \pm 0.34 \times 10^3$
1	$1.78 \pm 0.29 \times 10^4$	$4.44 \pm 0.15 \times 10^4$
2	$2.02 \pm 0.18 \times 10^4$	$4.78 \pm 0.08 \times 10^4$
3	$2.17 \pm 0.17 \times 10^4$	$4.92 \pm 0.06 \times 10^4$
4	$1.86 \pm 0.26 \times 10^4$	$4.51 \pm 0.13 \times 10^4$

750 nm. Upon addition of test compounds to CT DNA pretreated with EB ([DNA]/[EB] = 1) caused reduction in the emission intensity (Fig. S5). The quenching extents of the complexes were evaluated qualitatively by employing Stern–Volmer equation (2). From the obtained values it is inferred that EB was replaced by the compounds from the EB–DNA system (Fig. 7 and Table 3). Such a characteristic change is often observed in intercalative DNA interactions [40].

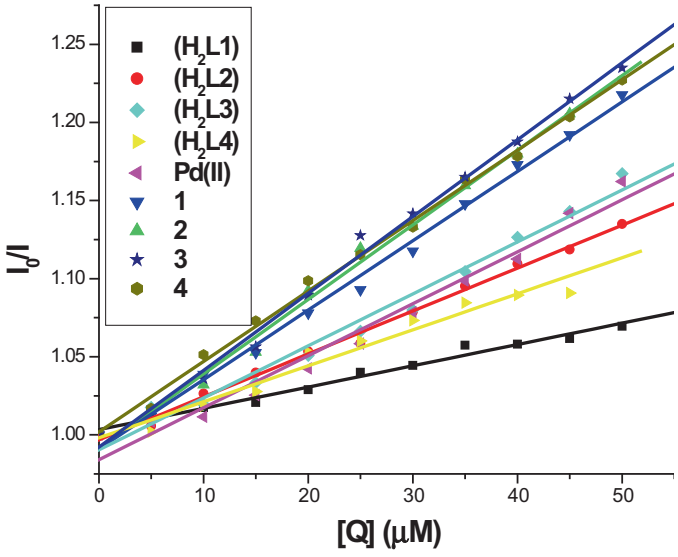

Fig. 7. Stern–Volmer plots of the EB–DNA fluorescence titration for compounds.

3.5. BSA binding studies

Serum albumin (SA) is the most abundant protein in plasma and is capable of binding, transporting and delivering an extraordinarily diverse range of endogenous and exogenous compounds like fatty acids, nutrients, steroids, certain metal ions, hormones and a variety of therapeutic drugs [41–43] in the blood stream to their target organs [44]. Because of its structural homology with human serum albumin (HSA), bovine serum albumin (BSA) has been most extensively studied. Binding to these proteins may lead to loss or enhancement of the biological properties of the original drug, or provide paths for drug transportation. In order to find out the binding of our compounds with BSA, the binding experiments were

carried out by using the **Pd(II)**, (**H_2L1**–**H_2L4**) and new complexes **1**–**4**. In all the experiments the concentration of BSA was kept constant at 10 μM and the concentration of test compounds was varied from 0–50 μM.

3.5.1. UV absorption spectra of BSA

A common method to distinguish between static and dynamic quenching is by careful examination of the absorption spectra of the BSA in the presence of complexes [45]. The UV absorption spectra of BSA in the presence of nine compounds (Fig. S6) showed that the absorption intensity of BSA was decreased with the addition of these compounds from 248 to 250 nm. The changes in the absorbance spectra for BSA + compounds indicate that test compounds interact with the BSA [46]. It is well known that dynamic quenching only affects the excited state of fluorophore and does not change the absorption spectrum. However, the formation of non-fluorescence ground-state complex induced the change in absorption spectrum of fluorophore. Thus, possible quenching mechanism of BSA by compounds was found as static quenching [47].

3.5.2. Fluorescence quenching studies of BSA

In order to get more information on the binding of the compounds with BSA, fluorescence spectrum of BSA was studied upon the addition of the test compounds. Though BSA contains three fluorophores, namely, tryptophan, tyrosine, and phenylalanine, the intrinsic fluorescence of BSA is mainly due to tryptophan alone, because phenylalanine has a very low quantum yield and the fluorescence of tyrosine is almost quenched when it becomes ionized or near to an amino group, a carbonyl group, or a tryptophan residue [48]. Changes in the emission spectra of tryptophan are common in response to protein conformational transitions, subunit associations, substrate binding, or denaturation. Hence, the interaction of BSA with our compounds was studied by fluorescence measurement at room temperature and the binding constants of the compounds were calculated. In a typical experiment, the fluorescence spectra were recorded in the range of 290–500 nm upon excitation at 280 nm. On increasing the concentration of compounds, a progressive decrease in the fluorescence intensity was observed, accompanied with a blue shift (Fig. S7). The observed blue shift may be due to the binding of compounds with the active site in BSA [49]. The binding constant K_{SV} value was obtained from the plot of I_0/I_{corr} versus [Q] in Stern–Volmer equation (3) (Fig. 8 and Table 4). The observed linearity in the plots indicated the ability of the complexes to quench the emission intensity of BSA. From K_{SV} values, it is seen that the new complexes **1**–**4** exhibited strong protein-binding ability with enhanced hydrophobicity than **Pd(II)** and (**H_2L1**–**H_2L4**) and this result reliable with their strong DNA binding affinity.

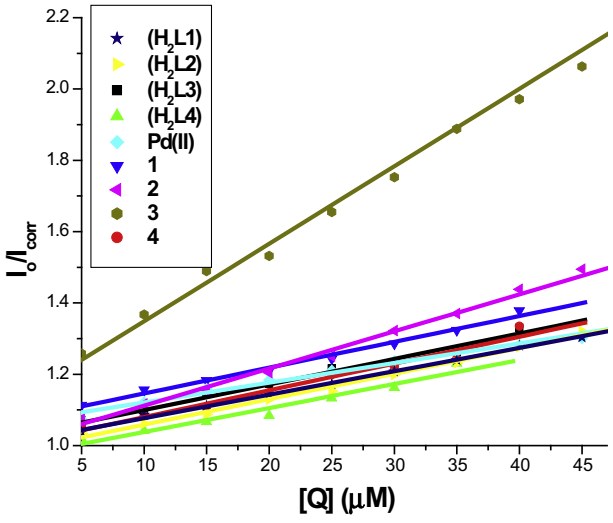

Fig. 8. Stern–Volmer plot.

Table 4
Quenching constant (K_{sv}), binding constant (K_{bin}) and number of binding sites (n) for the interactions of compounds (**1**–**4**) with BSA.

Complex	K_{sv} (M^{-1})	K_{bin} (M^{-1})	n
(**H_2L1**)	$6.57 \pm 0.48 \times 10^3$	$6.45 \pm 0.42 \times 10^4$	0.97
(**H_2L2**)	$7.10 \pm 0.37 \times 10^3$	$9.47 \pm 0.06 \times 10^4$	1.01
(**H_2L3**)	$7.16 \pm 1.33 \times 10^3$	$9.81 \pm 0.33 \times 10^4$	1.03
(**H_2L4**)	$6.70 \pm 0.45 \times 10^3$	$7.44 \pm 0.12 \times 10^4$	0.98
Pd(II)	$6.53 \pm 0.68 \times 10^3$	$6.29 \pm 0.04 \times 10^4$	0.96
1	$7.24 \pm 0.27 \times 10^4$	$1.64 \pm 0.35 \times 10^5$	1.07
2	$8.10 \pm 0.21 \times 10^4$	$3.19 \pm 0.26 \times 10^5$	1.17
3	$9.17 \pm 1.63 \times 10^4$	$3.46 \pm 0.23 \times 10^5$	1.23
4	$7.51 \pm 3.04 \times 10^4$	$1.79 \pm 0.31 \times 10^5$	1.12

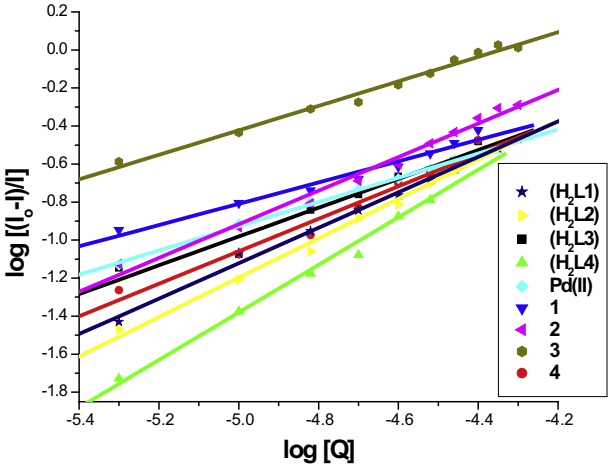

Fig. 9. Scatchard plot.

3.5.3. Binding constants and the number of binding sites

For the static quenching interaction, if it is assumed that there are similar and independent binding sites in the biomolecule, the binding constant (K_b) and the number of binding sites (n) can be determined according to the Scatchard equation (5) [30] (Fig. 9 and Table 4). The values of n at room temperature are approximately equal to 1, which indicates that there is just one single binding site in BSA for all the compounds.

3.5.4. Synchronous fluorescence spectroscopic studies of BSA

Synchronous fluorescence spectral study was used to obtain information about the molecular environment in the vicinity of the fluorophore moieties of BSA [50]. Synchronous fluorescence spectra show tyrosine residues of BSA only at the wavelength interval $\Delta\lambda$ of 15 nm whereas tryptophan residues of BSA at $\Delta\lambda$ of 60 nm. The concentration of complexes (0–50 μM) added to BSA (10 μM) is increased, a decrease in the fluorescence intensity with a blue shift in the tryptophan emission maximum is observed for all the complexes (Fig. S8). In contrast, the emission intensity of tyrosine residue increases without any change in the wavelength of emission. These observations indicate that the test compounds did not affect the microenvironment of tyrosine residues during the binding process significantly but the tryptophan microenvironment to a larger extent.

4. Conclusion

The present part describes the synthesis of four new palladium(II) arsine complexes containing 3-methoxysalicylaldehyde-4(*N*)-substituted thiosemicarbazones. All the new complexes have been characterized by using various spectroscopic techniques. *N*-methyl and *N*-ethyl substituted thiosemicarbazones yielded palladium complexes (**2**, **3**) with the NS chelation by forming a stable five member ring with N(1) hydrazinic nitrogen and thiolate sulfur atoms. However, the unsubstituted and *N*-phenyl substituted thiosemicarbazones yielded, ONS chelate (**1**, **4**) with the formation of five and six member rings by utilizing phenolic oxygen, N(1) nitrogen and thiolate sulfur atoms. Among them, complexes **2**–**4** have been characterized by X-ray crystallography. Further, the complexes (**1**–**4**), precursor complex $[PdCl_2(AsPh_3)_2]$ (**Pd(II)**) and their respective ligands ((**H_2L1**–**H_2L4**) have been subjected to test their DNA and protein binding efficacy. From the results it is observed that the test compounds significantly bind to the DNA and BSA. While comparing the binding ability of compounds with CT DNA/BSA, the new palladium(II) complexes (**1**–**4**) had better binding ability than their respective ligand and their parent complex $[PdCl_2(AsPh_3)_2]$ and among them complex **3** exhibited better binding activity.

Acknowledgment

The authors gratefully acknowledge Council of Science and Industrial research (CSIR), New Delhi, India and Department of Science and Technology DST, New Delhi, India for the financial support.

Appendix A. Supplementary data

CCDC 968809, 968810 and 968808 contain the supplementary crystallographic data for [Pd(H-Msal-mtsc)Cl($AsPh_3$)](**2**), [Pd(H-Msal-etsc)Cl($AsPh_3$)](**3**) and [Pd(Msal-ptsc)($AsPh_3$)](**4**), respectively. These data can be obtained free of charge via http://www.ccdc.cam.ac.uk/conts/retrieving.html, or from the Cambridge Crystallographic Data Centre, 12 Union Road, Cambridge CB2 1EZ, UK; fax: (+44) 1223-336-033; or e-mail: deposit@ccdc.cam.ac.uk. Packing diagram of the unit cell for complex **2** (Fig. S1); Packing diagram of the unit cell for complex **3** (Fig. S2); Packing diagram of the unit cell for complex **4** (Fig. S3); Absorption titration spectra of Starting material $[PdCl_2(AsPh_3)_2]$ (**Pd(II)**) and ligands (**H2L1**–**H2L4**) (Fig. S4); The emission spectra of the DNA–EB system (λ_{exc} = 515 nm, λ_{em} = 530–750 nm), in the presence of starting material **Pd(II)**, ligands (**H2L1**–**H2L4**) and new complexes **1**–**4** (Fig. S5); UV absorption spectra of BSA (10 μM) in the absence and presence of compounds (10 μM) (Fig. S6); The emission spectra of BSA in the presence of starting material **Pd(II)**, ligands (**H2L1**–**H2L4**) and new complexes **1**–**4** (Fig. S7); Synchronous spectra of BSA (1 μM) in the presence of increasing amounts of The emission spectra of the DNA–EB system (λ_{exc} = 515 nm, λ_{em} = 530–750 nm), in the presence of Starting material **Pd(II)**, ligands (**H2L1**–**H2L4**) and new complexes **1**–**4** for a wavelength difference of $\Delta\lambda$ = 60 nm. (Fig. S8). Supplementary data associated with this article can be found, in the online version, at http://dx.doi.org/10.1016/j.poly.2014.02.011.

References

[1] L.S. Sarma, J.R. Kumar, K.J. Reddy, A.K. Kumar, A.V. Reddy, Anal. Sci. 18 (2002) 1257.
[2] X.B. Yang, Q. Wang, Y. Huang, P.H. Fu, J.S. Zhang, R.Q. Zeng, Inorg. Chem. Commun. 25 (2012) 55.
[3] A. Castineiras, N.F. Hermida, I.G. Santos, L.G. Rodriguez, Dalton Trans. 41 (2012) 13486.
[4] A. Buschini, S. Pinelli, C. Pellacani, F. Giordani, M.B. Ferrari, F. Bisceglie, M. Giannetto, G. Pelosi, P. Tarasconi, J. Inorg. Biochem. 103 (2009) 666.
[5] J.L. Butour, S. Wimmer, F. Wimmer, P. Castan, Chem. Biol. Inter. 104 (1997) 165.
[6] A.C.F. Caires, Anti-Cancer Agents Med. Chem. 7 (2007) 484.
[7] J. Ruiz, J. Lorenzo, C. Vicente, G. López, J.M. López-de-Luzuriaga, M. Monge, F.X. Avilés, D. Bautista, V. Moreno, A. Laguna, Inorg. Chem. 47 (2008) 6990.
[8] P. Ńtarha, Z. Trávníček, I. Popa, J. Inorg. Biochem. 103 (2009) 978.
[9] M. Juribańić, K. Molčanov, B. Kojić-Prodić, L. Bellotto, M. Kralj, F. Zani, L. Tuńek-Božić, J. Inorg. Biochem. 105 (2011) 867.
[10] P.I.da S. Maia, A. Graminha, F.R. Pavan, C.Q.F. Leite, A.A. Batista, D.F. Back, E.S. Lang, J. Ellena, S.de.S. Lemos, H.S.S.de. Araujo, V.M. Deflon, J. Braz. Chem. Soc. 21 (2010) 1177.
[11] S.A. Khan, M. Yusuf, Eur. J. Med. Chem. 44 (2009) 2270.
[12] I. Kizilcikli, Y.D. Kurt, B. Akkurt, A.Y. Genel, S. Birteksoz, G. Otuk, B. Ulkuseven, Folia Microbiol. 52 (2007) 15.
[13] L. Otero, M. Vieites, L. Boiani, A. Denicola, C. Rigol, L. Opazo, C.O. Azar, J.D. Maya, A. Morello, R.L. Krauth-Siegel, O.E. Piro, E. Castellano, M. Gonzalez, D. Gambino, H. Cerecetto, J. Med. Chem. 49 (2006) 3322.
[14] S. Sharma, S.K. Singh, M. Chandra, D.S. Pandey, J. Inorg. Biochem. 99 (2005) 458.
[15] C. Metcalfe, J.A. Thomas, Chem. Soc. Rev. 32 (2003) 215.
[16] R. Prabhakaran, S.V. Renukadevi, R. Karvembu, R. Huang, J. Mautz, G. Huttner, R. Subhaskumar, K. Natarajan, Eur. J. Med. Chem. 43 (2008) 268.
[17] P. Kalaivani, R. Prabhakaran, E. Ramachandran, F. Dallemer, G. Paramaguru, R. Renganathan, P. Poornima, V. Vijaya Padma, K. Natarajan, Dalton Trans. 41 (2012) 2486.
[18] P. Kalaivani, R. Prabhakaran, F. Dallemer, P. Poornima, E. Vaishnavi, E. Ramachandran, V. Vijaya Padma, R. Renganathan, K. Natarajan, Metallomics 4 (2012) 101.
[19] P. Kalaivani, R. Prabhakaran, M.V. Kaveri, R. Huang, R.J. Staples, K. Natarajan, Inorg. Chim. Acta 405 (2013) 415.
[20] R. Prabhakaran, P. Kalaivani, R. Huang, P. Poornima, V. Vijaya Padma, K. Natarajan, Bio. Org. Med. Chem. 21 (2013) 6742.
[21] S. Purohit, A.P. Koley, L.S. Prasad, P.T. Manoharan, S. Ghosh, Inorg. Chem. 28 (1989) 3735.
[22] J.L. Burmeister, F. Basolo, Inorg. Chem. 3 (1964) 1587.
[23] A.I. Vogel, Text Book of Practical Organic Chemistry, fifth ed., Longman London, 1989. p. 268.
[24] (a) R.H. Blessing, Acta Crystallogr., Sect. A 51 (1995) 33;
(b) R.H. Blessing, Cryst. Rev. 1 (1987) 3;
(c) R.H. Blessing, J. Appl. Crystallogr. 22 (1989) 396.
[25] G.M. Sheldrick, SHELXTL Version 5.1, An Integrated System for Solving, Refining and Displaying Crystal Structures from Diffraction Data, Siemens Analytical X-ray Instruments, Madison, WI, 1990.
[26] G.M. Sheldrick, **shelxl**-97, A Program for Crystal Structure Refinement Release 97-2, Institut fur Anorganische Chemie der Universitat Gottingen, Tammanstrasse 4, D-3400, Gottingen, Germany, 1998.
[27] A. Wolfe, G.H. Shimer, T. Meehan, Biochemistry 26 (1987) 6392.
[28] G. Cohen, H. Eisenberg, Biopolymers 8 (1969) 45.
[29] M. van de Weert, L. Stella, J. Fluoresc. 20 (2010) 625.
[30] M. Jiang, M.X. Xie, D. Zheng, Y. Liu, X.Y. Li, X. Chen, J. Mol. Struct. 692 (2004) 71.
[31] R. Prabhakaran, P. Kalaivani, R. Jayakumar, M. Zeller, A.D. Hunter, S.V. Renukadevi, E. Ramachandran, K. Natarajan, Metallomics 3 (2011) 42.
[32] R. Prabhakaran, C. Jayabalakrishnan, V. Krishnan, K. Pasumpon, D. Sukanya, H. Bertagnolli, K. Natarajan, Appl. Organomet. Chem. 20 (2006) 203.
[33] R. Prabhakaran, R. Karvembu, T. Hashimoto, K. Shimizu, K. Natarajan, Inorg. Chim. Acta 358 (2005) 2093.
[34] R. Prabhakaran, S.V. Renukadevi, R. Karvembu, R. Huang, M. Zeller, K. Natarajan, Inorg. Chim. Acta 361 (2008) 2547.
[35] (a) Y.P. Tiam, C.Y. Duan, Z.L. Lu, X.Z. You, Polyhedron 15 (1996) 2263;
(b) S. Dey, V.K. Jain, A. Kwoedler, W. Kaim, Ind. J. Chem. 42A (2003) 2339.
[36] D.M. Boghaei, S. Mohebi, J. Chem. Res. (2001) 224.
[37] T.S. Lobana, A. Sanchez, J.S. Casas, A. Castineiras, J. Sordo, M.S. Garciaasende, E.M. Vazquez-Lopez, Dalton Trans. (1997) 4289.
[38] F. Basuli, M. Ruf, C.G. Pierpont, S. Bhattacharya, Inorg. Chem. 37 (1998) 6113.
[39] Z.C. Liu, B.D. Wang, Z.Y. Yang, Y. Li, D.D. Qin, T.R. Li, Eur. J. Med. Chem. 44 (2009) 4477.
[40] M. Chauhan, F. Arjmand, K. Banerjee, Inorg. Chem. 46 (2007) 3072.
[41] K. Yamasaki, T. Maruyama, U. Kragh-Hansen, M. Otagiri, Biochim. Biophys. Acta 1295 (1996) 147.
[42] X.M. He, D.C. Carter, Nature 358 (1992) 209.
[43] I. Sjoholm, B. Ekman, A. Kober, I. Ljungstedt-Pahlman, B. Seiving, T. Sjodin, Mol. Pharmacol. 16 (1979) 767.
[44] N. Ibrahim, H. Ibrahim, S. Kim, J.P. Nallet, F.O. Nepveu, Biomacromolecules 11 (2010) 3341.
[45] Y.J. Hu, Y. Liu, J.B. Wang, X.H. Xiao, S.S. Qu, J. Pharm. Biomed. Anal. 36 (2004) 915.
[46] Y.Y. Yue, X.G. Chen, J. Qin, X.J. Yao, Dyes Pigm. 79 (2008) 176.
[47] H.Y. Liu, Z.H. Xu, X.H. Liu, Chem. Pharm. Bull. 57 (2009) 1237.
[48] A. Sulkowska, J. Mol. Struct. 614 (2002) 227.
[49] Y. Wang, H. Zhang, G. Zhang, W. Tao, S. Tang, J. Lumin. 126 (2007) 211.
[50] N. Wang, L. Ye, B.Q. Zhao, J.X. Yu, Braz. J. Med. Biol. Res. 41 (2008) 589.